PHYSICAL REVIEW C **78**, 021304(R) (2008)

Persistence of the $N = 50$ shell closure in the neutron-rich isotope ^{80}Ge

H. Iwasaki,[1,*] S. Michimasa,[2] M. Niikura,[2] M. Tamaki,[2] N. Aoi,[3] H. Sakurai,[3] S. Shimoura,[2] S. Takeuchi,[3] S. Ota,[4] M. Honma,[5] T. K. Onishi,[1] E. Takeshita,[3] H. J. Ong,[1] H. Baba,[2] Z. Elekes,[6] T. Fukuchi,[7] Y. Ichikawa,[1] M. Ishihara,[3] N. Iwasa,[8] S. Kanno,[3] R. Kanungo,[3] S. Kawai,[7] T. Kubo,[3] K. Kurita,[7] T. Motobayashi,[3] A. Saito,[1] Y. Satou,[9] H. Suzuki,[1] M. K. Suzuki,[1] Y. Togano,[7] and Y. Yanagisawa[3]

[1]*Department of Physics, University of Tokyo, 7-3-1 Hongo, Bunkyo, Tokyo 113-0033, Japan*
[2]*Center for Nuclear Study (CNS), University of Tokyo, 7-3-1 Hongo, Bunkyo, Tokyo 113-0033, Japan*
[3]*RIKEN (The Institute of Physical and Chemical Research), 2-1 Hirosawa, Wako, Saitama 351-0198, Japan*
[4]*Department of Physics, University of Kyoto, Kitashirakawa, Kyoto 606-8502, Japan*
[5]*Center for Mathematical Sciences, University of Aizu, Tsuruga, Ikki-machi, Aizu-Wakamatsu, Fukushima 965-8580, Japan*
[6]*Institute of Nuclear Research of the Hungarian Academy of Sciences, P.O. Box 51, Debrecen H-4001, Hungary*
[7]*Department of Physics, Rikkyo University, 3-34-1 Nishi-Ikebukuro, Toshima, Tokyo 171-8501, Japan*
[8]*Department of Physics, Tohoku University, Aoba, Sendai, Miyagi 980-8578, Japan*
[9]*Department of Physics, Tokyo Institute of Technology, 2-12-1 Ookayama, Meguro, Tokyo 152-8551, Japan*

(Received 25 December 2006; revised manuscript received 25 May 2008; published 20 August 2008)

The 2_1^+ and 2_2^+ states of the neutron-rich isotope ^{80}Ge were studied by intermediate-energy heavy-ion scattering, providing for the first time the experimental value of $B(E2; 2_2^+ \rightarrow 0^+_{\text{g.s.}})$ for ^{80}Ge. The experimental data are well reproduced by large-scale shell model calculations, which suggest the important role of the proton particle-hole $2p_{3/2}$-$1f_{5/2}$ excitation in the configuration of the 2_2^+ state.

DOI: 10.1103/PhysRevC.78.021304 PACS number(s): 21.10.Re, 23.20.Js, 25.70.De, 27.50.+e

The advent of radioactive isotope (RI) beams gives access to exotic nuclei far from stability, where the proton-to-neutron ratios are drastically unbalanced. Collective properties of unstable even-even nuclei have been studied through the measurement of basic observables for probing quadrupole deformation, like the excitation energy $E(2_1^+)$ of the 2_1^+ state and the reduced $E2$ transition probability $B(E2; 2_1^+ \rightarrow 0^+_{\text{g.s.}})$ [1–7]. There is currently great interest in the properties of higher-lying states in exotic nuclei [4,8], such as the second 2_2^+ state and the yrast 4_1^+ state. The excitation energies and relevant $B(E2)$ of these states provide important information for classifying nuclear shapes as spherical vibrators, symmetric rotors, and asymmetric rotors [9], as well as information on seniority-type structure based on magicity [10].

The low-lying structure of Ge isotopes is known to show irregular trends along the long isotopic chain, characterized by prolate–oblate and spherical–deformed competition [7–12]. Close to the β-stability line, the energies of the yrast 2_1^+ and 4_1^+ states and nonyrast 2_2^+ state suggest a drastic shape transition of the Ge isotopes from nearly spherical ^{72}Ge to triaxial ^{76,78}Ge [9]. In the neutron-rich region, a smooth decrease in the $B(E2; 2_1^+ \rightarrow 0^+_{\text{g.s.}})$ values toward $N = 50$ has been reported recently [7]. However, the question of how the nuclear collectivity evolves in this neutron-rich region remains to be investigated, because experimental information on the higher-lying states beyond the 2_1^+ state is limited.

In this article, we report the first $B(E2)$ measurement for the $2_2^+ \rightarrow 0^+_{\text{g.s.}}$ transition of ^{80}Ge using a radioactive ^{80}Ge beam. Our aim is to observe the second members of the low-lying $E2$ states, such as 2_2^+ and 4_1^+, by means of intermediate-energy heavy-ion scattering. This can be demonstrated for heavier projectiles with $Z \geqslant 30$ [13], because the cross sections exciting the 2_2^+ and 4_1^+ states sharply rise as Z of the projectiles increases, due to the dominance of Coulomb excitation even at intermediate energies. Here, the 4_1^+ excitation mainly occurs via the two-step excitation. To demonstrate our method, we first performed measurements with a ^{76}Ge beam and compared the results. The structure of the neutron-rich ^{80}Ge isotope on the pathway to $N = 50$ is investigated by comparing our $B(E2)$ results to shell-model calculations performed with the most recent effective interaction [14].

The experiment was performed at the RIPS [15] facility in RI Beam Factory operated by RIKEN Nishina Center and CNS, University of Tokyo. The secondary Ge-isotope beam was produced by fragmentation of a 63 MeV/nucleon ^{86}Kr beam at around 100 pnA, with a 66.2-mg/cm^2-thick ^{9}Be target. Event-by-event measurements of magnetic rigidity ($B\rho$), time-of-flight (TOF), and energy loss (ΔE) allowed isotopic identification of the secondary beam as shown by the TOF versus ΔE plot in Fig. 1(a). A parallel-plate avalanche counter (PPAC) was set at the momentum dispersive focal plane of RIPS and used to measure $B\rho$. The TOF was determined by the timing difference between signals from the cyclotron frequency and from a 0.01-mm-thick plastic scintillator at the final focal plane of RIPS. ΔE was measured by a 0.1-mm-thick Si detector at the second focal plane of RIPS. The r.m.s. for the atomic (Z) and mass (A) identification were about 0.21 and 0.24, respectively, which were useful to remove beam contaminants. The intensities were around 1 kcps for ^{80}Ge and 6 kcps for ^{76}Ge, with $B\rho$ optimized for each isotope. The secondary beam was incident on a 175-mg/cm^2-thick Pb target. The average energy of the ^{76,80}Ge beams across the target was 37 MeV/nucleon. Two sets of

*Present address: Institut für Kernphysik, Universität zu Köln, Germany.

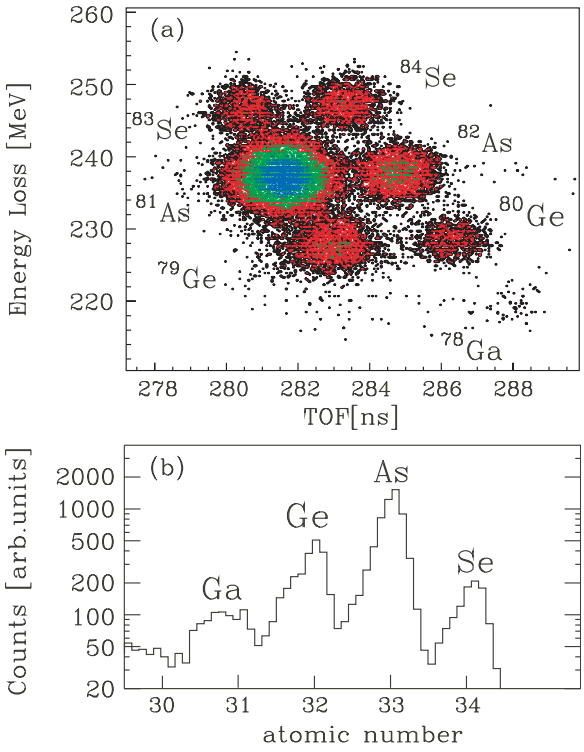

FIG. 1. (Color online) Example of particle identification plots for (a) the incoming beams and (b) the scattered particles in the ^{80}Ge setting. The linearized Z spectrum, which was made from the ΔE-E plot, is shown in (b) (see text).

PPACs were set before the Pb target to record the position and angle of the beam incident on the target. Possible background contributions were evaluated by a measurement with no target.

Scattered particles were detected by a Si telescope and a NaI(Tl) calorimeter located 75 cm and 1.5 m downstream of the secondary target, respectively. The Si telescope consisted of 16 silicon detectors placed in a 4×4 matrix. The size of each detector was 5×5 cm^2 and the thickness was 325 μm. The NaI(Tl) calorimeter [16] was composed of 132 NaI(Tl) crystals arranged in a 12×12 matrix except for three crystals at each corner. Each crystal had a volume of $31 \times 31 \times 50$ mm^3. The Z identification of the outgoing particles was then performed by the ΔE-E method, as shown by the linearized Z spectrum in Fig. 1(b). The resolution (r.m.s.) of the Z determination was around 0.17. The position information was determined by the segmentation of the NaI(Tl) calorimeter and was used to determine the scattering angle. The large size of the setup allowed to cover laboratory angles up to about 9.6°. This was useful to detect scattered particles from the two-step reaction leading to the higher-lying states like the 4_1^+ state, because such multistep reactions have maximum differential cross sections at large deflection angles [17]. On the other hand, Coulomb dominance in the reaction for the $E2$ excitation ensures reliable $B(E2)$ values over a wide range of scattering angles even close to the grazing angle, as demonstrated in Ref. [18]. In the present study, we obtained the angle-integrated cross section, which is defined as the differential cross section for the relevant inelastic reaction integrated over the detection angle up to 9.6°. The detection efficiency relevant to the angle-integrated cross section was mainly determined by the detector acceptance, because the efficiency in identifying Z of the scattered particles was high above 95%. The efficiency calculation was performed by a Monte Carlo simulation, which took into account the finite size and angular spread of the incident beam, the multiple scattering in the secondary target, and the detector geometry. Based on the simulation, the particle detection efficiency was found to be around 60–70% at laboratory scattering angles of less than 8.0°, while it suddenly decreases to 0% at 10.0° [19]. The overall efficiency was found to be 64 ± 4% for the ^{78,80}Ge + Pb scattering.

Deexcitation γ rays were detected by a DALI2 array [20] comprised of 158 NaI(Tl) detectors. The efficiencies for the γ rays emitted from the Ge beams in flight were simulated by the GEANT code [21]. The γ-ray asymmetry was estimated using the ECIS code mentioned later and incorporated in the calculation. The correction was found to be small (at most 5%) due to the large solid angle of the array. The overall full-energy-peak efficiencies were calculated to be 22 and 13%, respectively, for the 1- and 2-MeV γ rays. The spectral shape of γ rays was also simulated and used as a fitting function in deducing the γ-ray yield from a measured spectrum. The uncertainty in the efficiency calculation was estimated to be 5% based on the comparison between the simulated and measured values for γ rays from standard ^{22}Na, ^{60}Co, and ^{137}Cs sources.

First, we tested the performance of the experimental method by studying the reaction of the ^{76}Ge beam and comparing the $B(E2)$ results with the values of Ref. [22]. Figure 2(a) shows the Doppler-corrected, background-subtracted γ-ray energy spectrum observed for the ^{76}Ge + Pb reaction. The γ-ray peak, corresponding to the $2_1^+ \rightarrow 0_{\text{g.s.}}^+$ transition in ^{76}Ge, is evident at 569(7) keV. In the following, we cite the energies measured in this work, which are consistent with the previously measured values [22]. Figure 2(b) shows a γ-γ spectrum gated with 569-keV γ rays. A γ-ray peak is clearly seen at 855(9) keV corresponding to the $4_1^+ \rightarrow 2_1^+$ transition in ^{76}Ge. The γ-ray energy for the $2_2^+ \rightarrow 2_1^+$ transition was too close to that for the $2_1^+ \rightarrow 0_{\text{g.s.}}^+$ transition to be identified in the γ-γ spectrum. Hence, to observe the decay from the 2_2^+ state, we produced a sum-energy spectrum, Fig. 2(c), by adding the energies of two γ rays measured in coincidence. In Fig. 2(c), the transition from the 2_2^+ state is evident at 1109(12) keV, together with the minor peak at around 1400 keV for the 4_1^+ transition. The peak at 1109 keV includes the sum of two full-energy peaks for the $2_2^+ \rightarrow 2_1^+$ and $2_1^+ \rightarrow 0_{\text{g.s.}}^+$ transitions, as well as the Compton-scattering event from the $2_2^+ \rightarrow 0_{\text{g.s.}}^+$ transition, which gives two γ-ray signals. Another peak close to the threshold of 500 keV is attributed to the transition from the 2_1^+ state. In all the spectra, we chose true-timing events by gating the timing information from the NaI(Tl) γ-ray detectors. The width of the timing gate was set to be 10 ns. Accidental-coincidence contributions, which were main backgrounds in the present measurement, were estimated by setting a gate at the region beside the true coincidence event and were subtracted. The representative background spectrum is shown by the grey histogram in Fig. 2(b). The other background contributions, which were estimated but found to

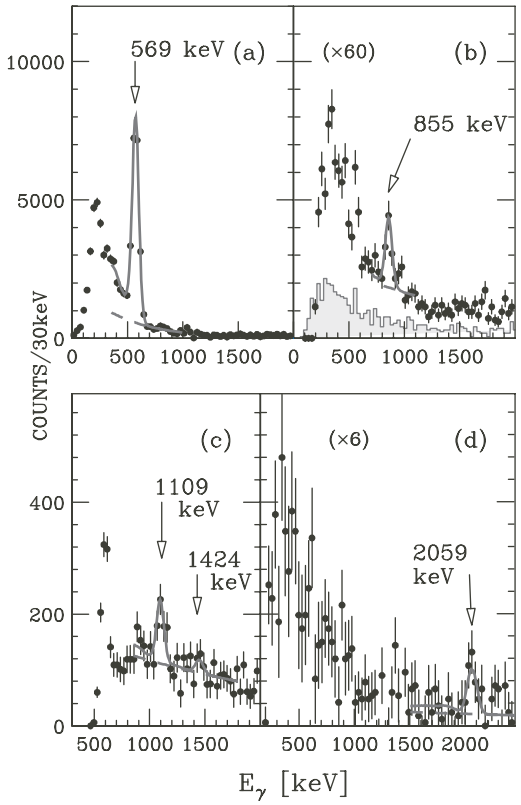

FIG. 2. Doppler-corrected γ-ray energy spectra observed for the ^{76}Ge + Pb reaction: (a) single γ-ray spectrum, (b) γ-ray spectrum gated with the $2_1^+ \rightarrow 0_{g.s.}^+$ transition, (c) sum spectrum for two γ rays, (d) γ-ray spectrum observed in coincidence with the decay of the 2_2^+ state (see text). The solid curves show simulated spectra by the GEANT code including continuous backgrounds, shown by the dashed curves. The grey histogram in (b) represents the background contribution subtracted in the spectra.

be negligible from the no-target data, were also subtracted. In the present work, the multiplicity M for the γ-ray detection was recorded. The condition $M = 1$ was applied in Fig. 2(a), while Figs. 2(b) and 2(c) were obtained with $M = 2$. Employing M is useful for reducing possible uncertainties in deducing excitation cross sections due to feeding contributions from higher excited states. Such events tend to result in higher multiplicity events due to the large acceptance of the DALI2 array. On the other hand, due to the narrow timing gate for true events, the γ-ray multiplicities were not affected significantly by accidental coincidence with the background.

The yields of the observed γ rays were obtained by comparing the spectra to the GEANT simulations, as shown in Fig. 2. The yields were used to extract the cross sections $\sigma_{pop}(J^\pi)$ populating each state (J^π) after considering the detection efficiency for both γ rays and scattered particles. The results obtained were $\sigma_{pop}(2_1^+) = 1293(112)$ mb, $\sigma_{pop}(2_2^+) = 75(10)$ mb, and $\sigma_{pop}(4_1^+) = 26(8)$ mb. After considering feeding contributions from higher excited states, we obtained the excitation cross sections $\sigma_{exp}(J^\pi)$ as summarized in Table I. For the 2_1^+ state, 68(9) mb feeding contributions were estimated from $\sigma_{pop}(2_2^+)$ and $\sigma_{pop}(4_1^+)$. For the 2_2^+ state, we subtracted contributions from the 3182-keV state in ^{76}Ge. Figure 2(d) shows the γ-ray energy spectrum, which contains both the γ-γ spectrum $(M = 2)$ gated with the $2_2^+ \rightarrow 0_{g.s.}^+$ transition and the triple γ-coincidence spectrum $(M = 3)$ gated with the $2_2^+ \rightarrow 2_1^+$ transition and the $2_1^+ \rightarrow 0_{g.s.}^+$ transition. The γ-ray peak at 2059(17) keV is consistent with the 2073-keV transition from the 3182-keV state populating the 2_2^+ state in ^{76}Ge [22]. Based on this observation, we subtracted contributions of 32(6) mb to deduce $\sigma_{exp}(2_2^+)$. Note that the branching ratios for the γ decays as well as the γ-ray efficiencies for the different multiplicity events are taken into account in these analyses. The quoted errors for σ_{exp} include the ambiguities in the photo-peak yields as well as the systematic errors added in quadrature. The systematic errors mainly stem from uncertainties in the efficiency calculations for scattered particles (6%) and γ rays (5%) and possible contaminants in the beam identification (3%).

To extract the transition probability $B(E2)$, we performed distorted-wave calculations allowing multistep excitation by using the ECIS code [23] in a rotational model. We used the optical potential of the ^{86}Kr + ^{208}Pb reaction at 43 MeV/nucleon [24], because the difference in the reaction system is small. The ECIS calculation includes two deformation parameters, the Coulomb deformation parameter β_2^C and the nuclear deformation parameter β_2^N, where the former is directly related to $B(E2)$ as $\beta_2^C = 4\pi\sqrt{5 \times B(E2; 2^+ \rightarrow 0^+)}/3ZeR^2$. We used the same β_2 values for the Coulomb and nuclear excitations, because Coulomb dominance of the present reaction reduces ambiguities due to nuclear excitations, compared to the case for lighter nuclei [1,2]. The other assumption that the same deformation length was used for the Coulomb and nuclear excitations lead to the same results. $\beta_2 = 0.260(12)$ was obtained from the $\sigma_{exp}(2_1^+) = 1225(112)$ mb. We thus obtained $B(E2; 2_1^+ \rightarrow 0_{g.s.}^+) = 527(49)$ e^2 fm^4. In the same way, we found $\beta_2 = 0.047(6)$ for the 2_2^+ state, giving $B(E2; 2_2^+ \rightarrow 0_{g.s.}^+) = 17(5)$ e^2 fm^4. A similar analysis was also made by selecting small scattering angles below 4° to ensure pure Coulomb excitation. The results agree with the experimental $B(E2)$ values deduced above within errors. Possible uncertainty arising from the choice of the potential was examined by extracting the same quantities with a different parameter set from the ^{58}Ni + ^{208}Pb reaction at 17 MeV/nucleon [25]. The $B(E2)$ results were only 4% greater than the results obtained with the ^{86}Kr potential.

Possible interference from the single-step $(0_{g.s.}^+ \rightarrow 2_2^+)$ and the two-step $(0_{g.s.}^+ \rightarrow 2_1^+ \rightarrow 2_2^+)$ excitations in deducing the $B(E2; 2_2^+ \rightarrow 0_{g.s.}^+)$ was investigated by using ECIS in the asymmetric rotational model, considering all the coupling schemes between the $0_{g.s.}^+$, 2_1^+, and 2_2^+ states. The γ parameter was taken to be 27°, which well reproduces both $E(2_2^+)/E(2_1^+)$ and $B(E2; 2_2^+ \rightarrow 0_{g.s.}^+)/B(E2; 2_1^+ \rightarrow 0_{g.s.}^+)$ ratios in ^{76}Ge. The $B(E2)$ results do not change by more than 10%, which suggests small contributions from the two-step excitation for the 2_2^+ state.

For the 4_1^+ state, the rotational model was employed to deduce $B(E2; 4_1^+ \rightarrow 2_1^+)$, where the β_2 value corresponds to $\beta_2 = 4\pi\sqrt{7/2 \times B(\mathrm{E2}; 4^+ \rightarrow 2^+)}/3ZeR^2$. From $\sigma_{exp}(4_1^+) = 26(8)$ mb, we obtained $\beta_2 = 0.282^{+0.020}_{-0.025}$, corresponding to

TABLE I. Measured energies and excitation cross sections for the 2_1^+, 2_2^+, and 4_1^+ states in ^{76}Ge and for the 2_1^+ and 2_2^+ states in ^{80}Ge. The present $B(E2)_{\rm exp}$ values in e^2 fm^4 are listed for the 2_1^+, $2_2^+ \to 0^+_{\rm g.s.}$ and $4_1^+ \to 2_1^+$ transitions and compared with the previous data $B(E2)_{\rm ref}$ [22] and the shell-model calculations $B(E2)_{\rm thr}$.

$^A Z$	J^π	E_x (keV)	$\sigma_{\rm exp}$ (mb)	$B(E2)_{\rm exp}$	$B(E2)_{\rm ref}$	$B(E2)_{\rm thr}$
^{76}Ge	2_1^+	569(7)	1225(112)	527(53)	554(19)	474
	2_2^+	1109(12)	43(12)	17(5)	17(4)	7
	4_1^+	1424(14)	26(8)	890^{+180}_{-190}	726(172)	650
^{80}Ge	2_1^+	662(7)	469(52)	200(26)	278(54)	256
	2_2^+	1579(15)	59(19)	23(7)	–	20

$B(E2; 4_1^+ \to 2_1^+) = 890^{+130}_{-150}$ e^2 fm^4. Due to the dominance of the two-step $E2$ excitation populating the 4_1^+ state, the β_4 value did not affect the result significantly (for example, the $B(E2)$ result changes by 13% if β_4 is taken to be 0.06 as suggested for ^{70,72}Ge [26]).

The $B(E2)$ values thus obtained for the 2_1^+, 2_2^+, and 4_1^+ states in ^{76}Ge are listed in Table I. After taking account of additional uncertainties due to the choice of the optical potential (4%), and the interference of the single-step and two-step excitations (10 and 13%, respectively, for the 2_2^+ and 4_1^+ states), we adopted $B(E2; 2_1^+ \to 0^+_{\rm g.s.}) = 527(53)$ e^2 fm^4, $B(E2; 2_2^+ \to 0^+_{\rm g.s.}) = 17(5)$ e^2 fm^4, and $B(E2; 4_1^+ \to 2_1^+) = 890^{+180}_{-190}$ e^2 fm^4. The present results agree well with the previous $B(E2)$ results [22].

We next studied the reaction for the ^{80}Ge beam. Figure 3 shows γ-ray spectra for the ^{80}Ge beam for the (a) single-γ ($M = 1$) and (b) γ-γ ($M = 2$) conditions, where the latter was obtained by gating with the $2_1^+ \to 0^+_{\rm g.s.}$ transition in ^{80}Ge. The spectra clearly show a peak at 662(7) keV for the 2_1^+ state and a peak at 917(11) keV for the $2_2^+ \to 2_1^+$ transition, both of which are consistent with the known transitions in ^{80}Ge [22]. The γ transition from the 4_1^+ state at 1742 keV [22] is not visible because of the limited statistics in the present experiment. $\sigma_{\rm pop}(J^\pi)$ was obtained to be $\sigma_{\rm pop}(2_1^+) = 481(52)$ mb and $\sigma_{\rm pop}(2_2^+) = 59(19)$ mb. As summarized in Table I, we obtained $\sigma_{\rm exp}(J^\pi)$ after considering the feeding contributions. For the 2_1^+ state, a contribution of 12(4) mb was estimated from $\sigma_{\rm pop}(2_2^+)$. No significant feeding transition was observed for the 2_2^+ state. For example, the 1σ upper limit of 3.3 mb was obtained for the feeding contribution from the 3423.6-keV state in ^{80}Ge [22], which could contribute to the 2_2^+ population.

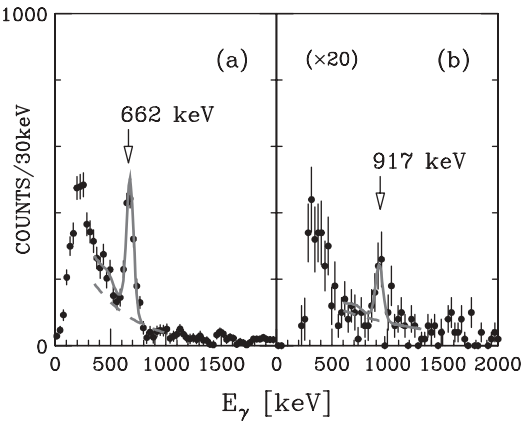

FIG. 3. Doppler-corrected γ-ray energy spectra observed for the ^{80}Ge + Pb reaction: (a) single γ-ray spectrum, (b) γ-ray spectrum gated with the $2_1^+ \to 0^+_{\rm g.s.}$ transition. The solid curves are fits to the data.

To deduce $B(E2)$, we followed the same procedure as that used in the ^{76}Ge analysis. The results of $\beta_2 = 0.155(9)$ and $0.053^{+0.008}_{-0.009}$ were obtained for the 2_1^+ and 2_2^+ states, respectively. We thus determined $B(E2; 2_1^+ \to 0^+_{\rm g.s.}) = 200(26)$ e^2 fm^4 and $B(E2; 2_2^+ \to 0^+_{\rm g.s.}) = 23(7)$ e^2 fm^4. For the first time, $B(E2; 2_2^+ \to 0^+_{\rm g.s.})$ has been determined. The present $B(E2; 2_1^+ \to 0^+_{\rm g.s.})$ is about 30% smaller, but still consistent within errors with the previous one (see Table I).

To understand the structure of ^{80}Ge, we performed the large-scale shell-model calculations using the JUN45 interaction, recently developed to describe nuclei around $A = 60$–100 [14]. The theoretical results of $B(E2)$ are shown in Table I. One states from the beginning that similar calculations for the lighter Ge isotopes are difficult to perform because of too large space dimensions [14]; the truncation of the configuration space will have the consequence of an unrealistic small collectivity that will underestimate the $B(E2)$ values. The model space includes the $2p_{3/2}$, $1f_{5/2}$, $2p_{1/2}$, and $1g_{9/2}$ orbits in addition to the ^{56}Ni core. The Hamiltonian parameters were obtained by modifying a renormalized G-matrix interaction through least-squares fits to 400 experimental binding and excitation energy data of 87 nuclei with $A = 63$–96 [14]. The diagonalization was performed using the code MSHELL [27]. We used the effective charges of $e_p = 1.5$ and $e_n = 1.0$ [14]. As shown in Table I, the present calculation describes the general trend of $B(E2)$ for ^{76}Ge fairly well, whereas the absolute values are smaller than the experimental data, which can be attributed to the insufficiency of the model space. On the other hand, the calculated $B(E2)$ values for ^{80}Ge are $B(E2; 2_1^+ \to 0^+_{\rm g.s.}) = 256$ e^2 fm^4 and $B(E2; 2_2^+ \to 0^+_{\rm g.s.}) = 20$ e^2 fm^4, showing good agreement with the present data. In the calculation, the proton and neutron $E2$ transition matrix elements A_p and A_n were calculated to be $(A_p, A_n) = (15.6, 12.3)$ and $(-7.3, 0.8)$, for the 2_1^+ and 2_2^+ states to the $0^+_{\rm g.s.}$ state, respectively. The relative weights of proton and neutron transitions are very different among the 2_1^+ and 2_2^+

states. The shell-model wave functions for the ground state and the 2_1^+ state are dominated by proton configurations $(1f_{5/2})^2(2p_{3/2})^2$ and $(1f_{5/2})^4$ (about 50% in total). In the 2_2^+ state, the main proton configurations are $(1f_{5/2})^2(2p_{3/2})^2$ and $(1f_{5/2})^3(2p_{3/2})^1$, where the latter is different from the $(1f_{5/2})^4$ configuration in the ground and 2_1^+ states by one particle-hole excitation. On the neutron side, the main configuration is $(1g_{9/2})^{-2}$, which dominates the neutron wave functions of the ground, 2_1^+, and 2_2^+ states (about 80%). The two $1g_{9/2}$ neutron-holes $(1g_{9/2})^{-2}$ are mostly coupled to 0^+ in the ground and 2_2^+ state, whereas in the 2_1^+ state they tend to be coupled to 2^+. The larger amplitude of the neutron $[(1g_{9/2})^{-2}]^{J=0^+}$ configuration for the 2_2^+ state compared to the 2_1^+ state results in the smaller contribution of $A_n = 0.8$ to the $2_2^+ \rightarrow 0^+_{\text{g.s.}}$ $E2$ transition. This can explain the suppressed neutron contribution A_n to the $E2$ strength of the $2_2^+ \rightarrow 0^+_{\text{g.s.}}$ transition. The agreement between the present results and the shell-model calculations that assume a restricted model space for neutrons suggests that the shell closure $N = 50$ persists in this neutron-rich region; in particular, for the presently studied ^{80}Ge nucleus, we reproduce the $B(E2)$ data without invoking the excitation above the $N = 50$ shell gap.

In summary, we have investigated the low-lying $E2$ states in the ^{76,80}Ge isotopes by means of γ-ray spectroscopy with intermediate-energy heavy-ion scattering. This technique gives access to excitations beyond the 2_1^+ state in neutron-rich nuclei, opening a new frontier for γ-ray studies with RI beams. The $B(E2; 2_2^+ \rightarrow 0^+_{\text{g.s.}})$ value for ^{80}Ge was measured for the first time. The data on ^{80}Ge are well understood in the framework of the large-scale shell model, which suggests a dominant role of the proton excitation for the $2_2^+ \rightarrow 0^+_{\text{g.s.}}$ transition of ^{80}Ge. The present shell model is still limited in space for lighter Ge isotopes like ^{76}Ge, while the model space is sufficient for describing the ^{80}Ge structure, suggesting the persistence of the $N = 50$ shell closure in this isotope.

We thank the RIKEN Ring Cyclotron staff for cooperation during the experiment. We also thank Professors. A. Gelberg, C. M. Petrache, and S. Franchoo for their valuable comments. This work was supported in part by a Grant-in-Aid for Young Scientists (B) No. 14740153 from MEXT, Japan. H.I. acknowledges support from the Alexander von Humboldt Foundation.

[1] T. Motobayashi *et al*., Phys. Lett. **B346**, 9 (1995).
[2] H. Iwasaki *et al*., Phys. Lett. **B522**, 227 (2001); H. Iwasaki *et al*., Phys. Lett. **B620**, 118 (2005) .
[3] T. Glasmacher, Annu. Rev. Nucl. Part. Sci. **48**, 1 (1998).
[4] F. Azaiez, Nucl. Phys. **A704**, 37c (2002).
[5] A. Bürger *et al*., Phys. Lett. **B622**, 29 (2005).
[6] O. Niedermaier *et al*., Phys. Rev. Lett. **94**, 172501 (2005).
[7] E. Padilla-Rodal *et al*., Phys. Rev. Lett. **94**, 122501 (2005).
[8] K. Starosta *et al*., Phys. Rev. Lett. **99**, 042503 (2007).
[9] W.-T. Chou, D. S. Brenner, R. F. Casten, and R. L. Gill, Phys. Rev. C **47**, 157 (1993).
[10] A. Makishima *et al*., Phys. Rev. C **59**, R2331 (1999).
[11] R. Lecomte *et al*., Phys. Rev. C **22**, 2420 (1980).
[12] J. Dobaczewski, W. Nazarewicz, J. Skalski, and T. Werner, Phys. Rev. Lett. **60**, 2254 (1988).
[13] H. Iwasaki *et al*., Eur. Phys. J. A **25**, Suppl. 1, 415 (2005).
[14] M. Honma, T. Otsuka, T. Mizusaki, and M. Hjorth-Jensen, J. Phys. Conf. Ser. **49**, 45 (2006).
[15] T. Kubo *et al*., Nucl. Instrum. Methods **B70**, 309 (1992).
[16] M. Tamaki *et al*., CNS-REP **59**, 76 (2003).
[17] K. Alder and A. Winther, Mat. Fys. Medd. K. Dan. Vidensk. Selsk. **32,** No. 8, 209 (1960).
[18] A. Gade *et al*., Phys. Rev. C **68**, 014302 (2003).
[19] The efficiency curve as a function of the scattering angle is available on request.
[20] S. Takeuchi *et al*., RIKEN Accel. Prog. Rep. **36**, 148 (2003).
[21] GEANT3, CERN program library.
[22] Evaluated Nuclear Structure Data File (ENSDF), http://www.nndc.bnl.gov/ensdf.
[23] J. Raynal, coupled-channel code ECIS97.
[24] P. Roussel-Chomaz *et al*., Phys. Lett. **B209**, 187 (1988).
[25] M. Beckerman *et al*., Phys. Rev. C **36**, 657 (1987).
[26] M. Kregar and B. Elbek, Nucl. Phys. **A93**, 49 (1967).
[27] T. Mizusaki, RIKEN Accel. Prog. Rep. **33**, 14 (2000).